Journal of Engineering Science and Technology
Vol. 17, No. 4 (2022) 2476 - 2495

REJECTION OF WING-ROCK MOTION IN DELTA WING AIRCRAFTS BASED ON OPTIMAL LADRC SCHEMES WITH BUTTERFLY OPTIMIZATION ALGORITHM

AHMED I. ABDUL-KAREEM[1], ALAQ F. HASAN[2], ARIF A. AL-QASSAR[1], AMJAD J. HUMAIDI[1*], RAAED F. HASSAN[3], IBRAHEEM KASIM IBRAHEEM[4], AHMAD TAHER AZAR[5,6]

[1]Control and Systems Engineering Department, University of Technology, Baghdad, Iraq
[2]Technical Engineering College, Middle Technical University, Baghdad, Iraq
[3]Electrical Engineering Technical College, Middle Technical University, Baghdad, Iraq
[4]Department of Computer Techniques Engineering, Dijlah University College, Baghdad 10001, Iraq
[5]College of Computer and Information Sciences, Prince Sultan University, Riyadh 11586, Saudi Arabia
[6]Faculty of Computers and Artificial Intelligence, Benha University, Benha 13518, Egypt
*Corresponding Author: amjad.j.humaidi@uotechnology.edu.iq

Abstract

This study presents control design based on Active Disturbance Rejection Control (ADRC) methodology to supress the effect of wing-rock motion in delta-wing aircraft. Two structures of ADRC have been addressed for the purpose of wing-rock motion rejection; one is based on Linear ADRC, and the other is based on Nonlinear ADRC. The setting of design parameters of designed ADRC controller is another problem, which has been solved by using modern optimization technique. This work has suggested Butterfly Optimization Algorithm (BOA) for tuning these design parameters in such a way an optimal performance of controller could be reached. A comparison study in performance between LADRC and NADRC has been conducted via numerical simulation show the superior of LADRC over the NADRC in terms of rejection capabilities. Moreover, the simulated results showed that the BOA could successfully improve the performance of proposed controller as compared to try-and-error procedure.

Keywords: Butterfly optimization algorithm, Delta-wing aircraft, Disturbance rejection, Linear ADRC, Nonlinear ADRC, Wing-rock motion.

1. Introduction

The coupling between the unsteady aerodynamic forces and aircraft dynamic response results in the rise of a self-sustaining limit-cycle oscillation (LCO). This oscillatory motion is commonly known as "wing rock" motion. When operating at high angles of attack, many aircrafts with slender plan-form undergo self-induced oscillatory rolling motion. Also, the nonlinear aerodynamic mechanisms are the other cause of wing rock motion at high angles of attack [1-5].

In general, the wing rock phenomenon can be originated due to aerodynamic conditions in the time of flight, or it can be caused by mechanical hysteresis such as backlash, cable stretching, dry Friction and hydraulic oil compressibility. Wing rock can also be caused by inherent mechanical hysteresis in the aircraft for example: in certain commercial aircraft the occurrence of wing rock is due to backlash in power transmission system [1].

A wide range of studies has also been conducted by researchers on aircraft exhibiting wing rock caused by aerodynamic hysteresis. It has been reported that some of the aircrafts that experience wing rock phenomenon include F-16 Fighting Falcon, F-4 Phantom, Gnat Trainer, F-18 Hornet, A-4 Skyhawk, F-14 Tomcat and Tornado. Owing to the different types of aircraft and different sources of primary physical mechanism responsible for the nonlinearities, the scope and problem of wing rock are also not very well understood. In general, it has been thought that wing rock motion is motivated by asymmetries of, which developed by negative roll damping and maintained by the nonlinear aerodynamic roll damping [1]. Figure 1 shows a sketch of subsonic flow field over the top surface of a delta-wing. It is clear from the figure that the wing-rock is generated due to the dynamic stall and the asymmetries of leading-edge vortices and fore-body vortices.

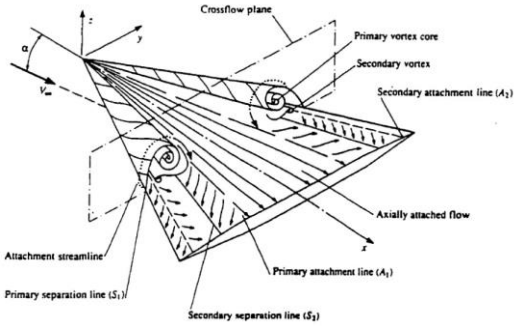

Fig. 1. The flow distribution over delta wing.

Wing rock motion may also be triggered due to sideslip, or it can occur during a zero sideslip flight with flow asymmetries over the aircraft flight at high angle of attacks. According to a study conducted on F-4 Phantom, it has been observed that when operated at high angle of attack the aircraft could undergo divergence behavior in pitch and yaw known as "nose slice". Preceding the nose slice, the aircraft would experience wing rock motion [1].

Wing rock depends on the details of the configuration geometry of the aircraft. To suppress the wing rock on al1 types of aircraft, the primary mechanism responsible for the wing rock must be identified. Due to the complexity of flow

fields for different aircraft, the identification of the exact causes and the source of primary mechanism could be difficult. To eliminate the aircraft configuration dependent effects, research has been devoted to slender delta wing model.

Wing rock motion is not acceptable from the operational and safety point of view. The problem is a concern to a pilot because it may have an adverse effect on aircraft maneuverability during landing approach or during a dogfight in a combat situation and it may lead to its crash [6]. The severity of wing rock may degrade the performance of weapon aiming control and accuracy.

Owing to the highly nonlinear nature of the flight dynamics, the problem of the wing rock is not very well understood. No satisfactory method has been developed to solve the problem. During the aerodynamic design stage of the aircraft, consideration can be taken to minimize the occurrence of the wing rock, such as the design with a slender body and highly swept wings, use of the roll damper, fore-body jet blowing etc. These conventional control methods may not be effective to control wing rock, which occurs at high angle of attack.

Advanced and nonlinear controllers have to be developed to cope with high nonlinearity and complexity due to wing rock phenomenon. In what follows, a literature of recent control research that fix and solve the wing-rock problem in aircrafts have been presented:

Kooi [1] had proposed dynamic recurrent neural network controller based on RBF (Radial Basis Function) for wing rock motion control in a test bed aircraft (WTI/F-16) with delta-wing configuration. Based on the input-output data gathered from wing rock behavior, the recurrent dynamic neural network structure is utilized for identification process by approximating the unknown nonlinearities in physical system.

Castellanos et al. [5] presented L1 adaptive control design to solve the stabilization problem due to wing rock phenomenon. The design of controller has been developed to ensure closed-loop stability in the presence of actuator dynamic and model uncertainties. It has been shown that the order of chosen filter, within the structure of L1 adaptive control, has direct effect on the performance of controlled system.

Ignatyev [6] proposed a neural network adaptive controller for suppressing the wing-rock motion for the scaled 3-DOF aircraft model mounted on a rig and maneuverers inside wind tunnel.

Gonz´alez and Ra´ul [7] presented direct adaptive control to stabilize and control strict feedback systems. The semi-global asymptotic stability has been proven under limited knowledge of system dynamics. The slender delta-wing rock phenomenon has been applied as a case study of this work.

Steven and .Svoboda [8] proposed dynamic recurrent radial basis function (DRRBF) for modeling the mechanical hysteresis, which is the main cause of wing-rock behavior in the aircraft. The adaptive control law has been developed to minimize a cost function in such a way to guarantee the controlled system stability.

Guglieri and Satori [9] proposed Sliding Mode Control (SMC) to suppress the effect of wing rock behavior by minimizing a cost function in terms of roll angular error and commanded input. The robustness of proposed controller has been verified in the presence of parametric disturbances.

Humaidi and Hameed [10] have presented three versions of controllers based on model reference adaptive control (MRAC) to control the rolling motion of Delta-Wing aircraft due to rock-wing dynamic in the presence of unmatched uncertainty. The proposed controllers are σ-modified MRAC, weighted σ-modified MRAC and classical MRAC. The proposed controllers are devoted. The numerical results showed that the weighted σ-modified controller outperforms the other controllers in terms of tracking error accuracy, robustness characteristics and control effort.

Liu and Su [11] presented a fuzzy logic control (FLC) design based on variable universe of discourse for wing-rock motion control. The proposed FL controller showed both high tracking precision and robustness against parametric uncertainty.

Al-Qassar et al. [12] presented finite-time control design based on Super Twisting Sliding Mode Control (STSMC) methodology to reduce the effect of wing-rock motion in delta-wing aircraft. The Whale Optimization Algorithm (WOA) has been used to tune the design parameters of proposed controller to improve the dynamic performance of controlled system.

Wu et al. [13] has proposed robust control scheme based on radial basis function (RBF) neural network structure and extended state observer (ESO). The study considered the input saturation problem by synthesizing an auxiliary system. The computer simulation showed the effectiveness of proposed wing rock control based on backstepping control law and improved ESO.

Roshanian and Rahimzadeh [14] presented the design of robust Model Reference Adaptive Control (MRAC) for single DOF motion of wing-rock dynamics. The general structure has been developed for stable adaptive laws, which guaranteed the asymptotic stability of controlled system with uniform bounded tracking of robust controller.

Humaidi et al. [15] presented a comparison study between two nonlinear control schemes to angle control of roll channel for delta-wing aircraft subjected to wing-rock behavior. The first proposed controller is based on sliding mode backstepping control, while the other is based on observer-based sliding mode control. The performance of proposed controllers has evaluated and compared in terms of their transient and robustness characteristics.

Active Disturbance Rejection Controller (ADRC) was firstly proposed by J. Han with nonlinear gains. The control design of ADRC focused on nonlinear systems and considered both uncertain dynamics and disturbances. The essential idea of ADRC is firstly to combine both internal uncertain dynamics and external disturbances into a total uncertainty and to then estimate this combined uncertainty by an extended state observer (ESO) and thereafter to be cancelled out using state feedback structure [16-24].

In the control design of ADRC for the motion rejection of wing-rock, some of design parameters appear. It has been shown that these design parameters have direct effect on performance of ADRC and hence on the dynamic performance of controlled plant [25-27].

Modern optimization technique will be used, instead of try-and-error procedure, to tune these design parameters in order to have optimal performance of controller. In this study, Butterfly Optimization Algorithm (BOA) to optimal tuning of design parameters. The butterfly optimization algorithm is a new algorithm firstly

proposed by Arora and Singh in 2019. The BOA is a nature-inspired algorithm, which simulates the mating behavior and foraging behavior of butterflies. The mechanism of this algorithm is based on smell sense to localize the mating partner or nectar [28-30]. The BOA has been effectively applied to solve many problems in various engineering applications [31-34].

The following points highlight the main contribution of this study:

- Design of active disturbance rejection control to supress the effect of wing-rock motion in Delta-Wing Aircraft.
- Design the observer of ADRC based on super-twisting sliding mode methodology.
- Tuning of design parameters by developing BOA to reach optimal performance of ADRC.
- Conducting a comparative study in performance between linear ADRC and nonlinear ADRC.

2. Dynamic Modelling of Wing-Rock Behaviour

Based on wind tunnel simulation, experimental tests are conducted to establish the dynamic model according to fitting models which mimic the behaviour of wing-rock. However, the dynamic models got from data-fitting techniques are described as nonlinear and second-order differential models. In addition, one model differs from other model in terms of nonlinearity parts.

If one degree of freedom (DOF) has been taken into account, the dynamic model describing wing-rock motion can be given by [35, 36]:

$$\ddot{\phi} = (\rho \,.\, U_{\infty}^{2}.S_b/2.\mathrm{I}_{xx})\, C_l + D.u \tag{1}$$

where, the variables ϕ and ρ represent roll angle and the air density, respectively.

The speed of free air stream is defined by U^{∞}, S defines the wing area of aircraft. The coefficients b denotes the wing chord. The wing moment of inertia around the roll span axis is denoted by I_{xx}, the position and effectiveness rolling of differential ailerons are represented by u and D, respectively. The parameter C_l can be expressed by [35-37]

$$C_l = a_1\phi + a_2.\dot{\phi} + a_3\,|\phi|.\dot{\phi} + a_4\,|\dot{\phi}|.\dot{\phi} + a_5.\phi^3 \tag{2}$$

where, the coefficients a_i, $i = 1, \ldots, 4$, are unknown constants. Combining Eqs. (1) and (2) to have

$$\ddot{\phi} = b_1.\phi + b_2.\dot{\phi} + b_3.|\phi|\,.\dot{\phi} + b_4\,\dot{\phi}\,|\dot{\phi}| + b_5.\phi^3 + b_6.u \tag{3}$$

Based on above equation, the state variable can be established by setting $x_1 = \phi$, $x_2 = \dot{x}_1 = \dot{\phi}$. This gives the following state variable equation

$$\begin{aligned} \dot{x}_1 &= x_2 \\ \dot{x}_2 &= b_1\,x_1 + b_2\,x_2 + b_3.x_2.|x_1| + b_4.x_2.|x_2| + x_1^3 + b_6.u \end{aligned} \tag{4}$$

where the coefficients b_1, b_2, b_3, b_4 and b_5 are also unknown constants.

If the disturbance or non-parametric uncertainty $\zeta(t)$, represented by wind and storm gust, has been added to the dynamic model, the following extended state variable is obtained

$$\dot{x}_1 = x_2$$
$$\dot{x}_2 = b_1 x_1 + b_2 x_2 + x_2(b_3|x_1| + b_4|x_2|) + b_5 {x_1}^3 + b_6 u + \zeta(t) \quad (5)$$

Remark 1**:** In order to ensure the stability of the Delta Wing Aircrafts, the value of c_2 must satisfy $c_2 > \delta > |\dot{\zeta}(t)|$.

3. ADRC for Delta Wing Aircrafts

The structure of Active Disturbance Rejection Control (ADRC) has three main elements: Tracking differentiator (TD), State-error-feedback (SEF) controller and extended state observer (ESO). The role of tracking differentiator is to perform differentiation of input signal corrupted with noise or spikes to quickly get the tracking signal. The ESO is utilized for estimation of extended state, which represents the lumped terms of external (disturbance) and internal uncertainties. Then, the control signal to realize rejection of wing-rock motion for delta-wing aircraft, is extracted based on nonlinear combination of estimator and SEF controller.

3.1. Tracking differentiator (TD)

The tracking differentiator is an essential part of ADRC structure which responsible for obtaining monotonic input profile under spiky or noisy set-point to be reasonably followed by plant output. The governing equations for TD can be developed as follows [25-27]:

For a double integral plant described by

$$\begin{cases} \dot{x}_1 = x_2 \\ \dot{x}_2 = u \end{cases} \quad (6)$$

where, the input is bounded $|u| \leq r$. If the signal v is assigned to desired value for x_1 and one can find the time-optimal solution according to

$$u = -r.sign\left(x_1 - v + \frac{x_2.|x_2|}{2r}\right) \quad (7)$$

Based on this principle, the solution of following differential equations will give the desired transient profile:

$$\begin{cases} \dot{v}_1 = v_2 \\ \dot{v}_2 = -r\ sign\left(v_1 - v + \frac{v_2|v_2|}{2r}\right) \end{cases} \quad (8)$$

where, the state variables v_1 and v_2 represents the tracking signal and its derivative of the desired trajectory, respectively.

The parameter r can be chosen to slow down or speed up the transient profile according to the physical limitations of certain application. Moreover, for real-time implementation, the discretization of continuous-time time-optimal solution described by Eq. (7) leads to rise of considerable numerical errors. To solve this problem, the double integral plant is discretized as follows

$$\begin{cases} v_1(k+1) = v_1(k) + h v_2(k) \\ v_2(k+1) = v_2(k) + h\ u \end{cases} \quad (9)$$

where h is the sampling period. The control signal is rewritten as

$$u = fst(v_1 - v, v_2, r_0, h_0) \quad (10)$$

where r_0 and h_0 are the design parameters of controller. The function $fst(v_1 - v, v_2, r_0, h_0)$ is defined by

$$fst(v_1 - v, v_2, r_0, h_0) = \begin{cases} -r_0\ sign(a), & a > d \\ -r_0\ \frac{a}{d}, & a \le d \end{cases} \tag{11}$$

$$a = \begin{cases} v_2 + \frac{a_o - d}{2}\ sign(y), & |y| > d_o \\ v_2 + \frac{y}{h_0}, & |y| \le d_o \end{cases} \tag{12}$$

$$\begin{cases} d = r_0 h_0 \\ d_o = d h_0 \\ a_o = \sqrt{d^2 + 8 r_0 |y|} \\ y = v_1 - v + h_0\ v_2 \end{cases} \tag{13}$$

The time-optimal solution, represented by Eq. (10), could ensure fastest rate of convergence, from v_1 to v without any overshoot.

3.2. Linear active disturbance control

3.2.1. Linear extended state observer

One can express the controlled nonlinear plant subjected to internal uncertainties and external disturbances by the following nonlinear equation [25-27]

$$\begin{cases} \dot{x}_1 = x_2 \\ \dot{x}_2 = f(x, w, t) + bu \\ y = x_1 \end{cases} \tag{14}$$

where, the input and output signals are defined by u and y, respectively. The function $f(x, w, t)$ represents the unknown nonlinear term with disturbance, and b denotes control input gain.

If the above state variable systems are extended to introduce a new state x_3 that lumps the total disturbances, nonlinearities and uncertainties, and expressed by $x_3 = f(x, w, t) + \Delta b\ u$, then Eq. (14) can be written as

$$\begin{cases} \dot{x}_1 = x_2 \\ \dot{x}_2 = x_3 + bu \\ \dot{x}_3 = g(t) \\ y = x_1 \end{cases} \tag{15}$$

One can propose the following state observer for the expanded system of Eq. (15) as follows:

$$\begin{cases} \dot{\hat{x}}_1 = \hat{x}_2 + \beta_1\ (x_1 - \hat{x}_1) \\ \dot{\hat{x}}_2 = \hat{x}_3 + b_0 u + \beta_2\ (x_1 - \hat{x}_1) \\ \dot{\hat{x}}_3 = \beta_3\ (x_1 - \hat{x}_1) \end{cases} \tag{16}$$

where $\hat{x}_1$, $\hat{x}_2$ and $\hat{x}_3$ are the estimated states of actual states x_1, x_2, and x_3 respectively. The parameters β_1, β_2 and β_3 are selected as $[\beta_1,\ \beta_2,\ \beta_3] = [3w_o,\ 3\ w_o^2,\ w_o^3]$ to ensure the stability of the ESO, where w_o represents the observer bandwidth [25-27].

Now, if the estimation errors define the differences between actual and estimated states, $\tilde{x}_1 = x_1 - \hat{x}_1$, $\tilde{x}_2 = x_2 - \hat{x}_2$ and $\tilde{x}_3 = x_3 - \hat{x}_3$, then Eq. (16) can be accordingly rewritten as follows:

$$\begin{cases} \dot{\tilde{x}}_1 = \dot{x}_1 - \dot{\hat{x}}_1 = -3w_o\,\tilde{x}_1 + \tilde{x}_2 \\ \dot{\tilde{x}}_2 = \dot{x}_2 - \dot{\hat{x}}_2 = -3w_o^2\,\tilde{x}_1 + \tilde{x}_3 \\ \dot{\tilde{x}}_3 = \dot{x}_3 - \dot{\hat{x}}_3 = -w_o^3\,\tilde{x}_1 + \dot{x}_3 \end{cases} \tag{17}$$

The state error $\tilde{X} = [\tilde{x}_1, \tilde{x}_2, \tilde{x}_3]^T$ is defined to rewrite Eq. (17) as:

$$\dot{\tilde{X}} = \boldsymbol{A}\,\tilde{X} + \boldsymbol{B}$$

$$\begin{bmatrix} \dot{\tilde{x}}_1 \\ \dot{\tilde{x}}_2 \\ \dot{\tilde{x}}_3 \end{bmatrix} = \begin{bmatrix} -3w_o & 1 & 0 \\ -3{w_o}^2 & 0 & 1 \\ -{w_o}^3 & 0 & 0 \end{bmatrix} \begin{bmatrix} \tilde{x}_1 \\ \tilde{x}_2 \\ \tilde{x}_3 \end{bmatrix} + \begin{bmatrix} 0 \\ 0 \\ \dot{x}_3 \end{bmatrix} \tag{18}$$

According to Eq. (18), it is always possible to select w_o in such a way that the eigenvalues of A are in the left-hand plane, by which it is possible to find a positive definite matrix P such that,

$$\boldsymbol{A}^T\boldsymbol{P} + \boldsymbol{P}\boldsymbol{A} = -\boldsymbol{Q} \tag{19}$$

for any given positive definite matrix $\boldsymbol{Q}$. Defining a Lyapunov candidate,

$$V = \tilde{X}^T P \tilde{X} \tag{20}$$

The time derivative of Eq. (20) is giving by

$$\dot{V} = \dot{\tilde{X}}^T P\tilde{X} + \tilde{X}^T P\dot{\tilde{X}}$$
$$\dot{V} = (A\tilde{X} + B)^T P\tilde{X} + \tilde{X}^T P\left(A\tilde{X} + B\right) = \tilde{X}^T A^T P\tilde{X} + \tilde{X}^T PA\tilde{X} + 2B^T P\tilde{X}$$
$$\dot{V} = -\tilde{X}^T Q\tilde{X} + 2B^T P\tilde{X}$$
$$\dot{V} \le -\eta(Q)\left\|\tilde{X}\right\|^2 + 2\varepsilon\|P\|\left\|\tilde{X}\right\|$$

After a sufficiently long time, the norm of the state error $\tilde{X}$ is bounded by

$$\left\|\tilde{X}\right\| \le \frac{2\varepsilon\|P\|}{\eta Q} \tag{21}$$

where η is the smallest eigenvalue of a matrix.

Lemma 1. Given a differentiable continuous function $\Upsilon(t)$ satisfying

$$\sigma_1 \le \Upsilon(t) \le \sigma_2 \tag{22}$$

with positive constant σ_1 and σ_2. The derivative $\Upsilon(t)$ is also bounded.
the estimation error of $\tilde{x}_3$ is bounded, and according to Lemma 1, the derivative of $\tilde{x}_3$ is bounded by,

$$\left|\dot{\tilde{x}}_3\right| < L \tag{23}$$

where L is a positive constant.

3.2.2. Linear state error feedback

State error feedback control law generates control signal u for system by using the error from the output of LESO and TD.

$$\begin{cases} e_1 = v_1 - \hat{x}_1 \\ e_2 = v_2 - \hat{x}_2 \end{cases} \tag{24}$$

A linear combination of error signal and its differential can be constructed as follows:

$$u_o = k_1 e_1 + k_2 e_2 \tag{25}$$

Feedback control law can be obtained as

$$u = \frac{u_o - \hat{x}_3}{b_0} \tag{26}$$

Definition 1. Let $x_i(t) \in (0 \le i \le n)$ and $\hat{x}_i(t) \in (0 \le i \le n+1)$ be the solutions of the closed-loop system Eq. (14) under the feedback Eq. (26) with LESO Eq. (16), coupling TD Eq. (9). Let $x_3 = f(x, w, t) + \Delta b u$ be the extended state variable. We say that the ADRC is convergent if, for any given initial values of Eqs. (5), (10), and (11), there exists a constant $R_O > 0$ such that for any $R > R_o$,

$$\lim_{\substack{t\to\infty \\ \varepsilon\to 0}} [x_i(t) - \hat{x}_i(t)] = 0\,, 0 \le i \le n+1 \tag{27}$$

$$\lim_{\substack{t\to\infty \\ \varepsilon\to 0}} [x_i(t) - z_i(t)] = 0\,, 0 \le i \le n \tag{28}$$

Moreover, for any given $\rho > 0$, $\lim_{R\to 0}[v_1(t) - v] = 0$ uniformly for $t \in [\rho, \infty)$.

3.3. Nonlinear active disturbance control

3.3.1. The super-twisting extended-state observer (STESO)

This study applies STESO to estimate the states x_1, x_2 and x_3. The mathematical structure of STESO is described by 3rd order dynamics as follows

$$\begin{cases} \dot{\hat{x}}_1 = \hat{x}_2 + \beta_1 . |x_1 - \hat{x}_1|^{\frac{2}{3}} . sgn(x_1 - \hat{x}_1) \\ \dot{\hat{x}}_2 = \hat{x}_3 + b_0 . u + \beta_2 \ |x_1 - \hat{x}_1|^{\frac{1}{3}} . sgn(x_1 - \hat{x}_1) \\ \dot{\hat{x}}_3 = \beta_3 \, . sgn(x_1 - \hat{x}_1) \end{cases} \tag{29}$$

The hyperbolic tangent nonlinear function has been used instead of signum function due its smooth characteristics, which in turn leads to considerably reduction of the chattering effect. As such, the term $\beta_3\ sgn(x_1 - \hat{x}_1)$ is replaced by $\beta_3 \tanh\big(c(x_1 - \hat{x}_1)\big)$ in Eq. (29), which can be rewritten as

$$\begin{cases} \dot{\hat{x}}_1 = \hat{x}_2 + \beta_1 . |x_1 - \hat{x}_1|^{\frac{2}{3}} . sgn(x_1 - \hat{x}_1) \\ \dot{\hat{x}}_2 = \hat{x}_3 + b_0 . u + \beta_2 . |x_1 - \hat{x}_1|^{\frac{1}{3}} . sgn(x_1 - \hat{x}_1) \\ \dot{\hat{x}}_3 = \beta_3 . \tanh\big(c(x_1 - \hat{x}_1)\big) \end{cases} \tag{30}$$

3.3.2. Nonlinear state error feedback (NSEF)

The nonlinear state error feedback element is configured by nonlinear combination of ESO and TD, that is;

$$\begin{cases} e_1 = v_1 - \hat{x}_1 \\ e_2 = v_2 - \hat{x}_2 \\ u_o = c_1\, fal(e_1, \alpha_1, \delta) + c_2\, fal(e_2, \alpha_2, \delta) \\ u = \frac{u_o - \hat{x}_3}{b_0} \end{cases} \tag{31}$$

where fal is a non-smooth function proposed by researcher Han. The fal function is defined by

$$fal = \begin{cases} e\,.\,\delta^{\alpha-1} & |e| \le \delta \\ |e|^{\alpha}.\,sgn(e) & |e| > \delta \end{cases} \tag{32}$$

where δ is threshold of non-smooth interval, α is control parameter. If $|e| < \delta$, a linear function fal is applied to avoid the high-frequency fluctuations due to sign function. In case of $|e| > \delta$, a non-smooth fal function is used with adjustable α parameter $(0 < \alpha < 1)$.

4. Butterfly Optimization Algorithm (BOA)

The butterfly optimization algorithm belongs to the family of metaheuristic algorithms. It is inspired by nature more precisely mimics the behaviour of butterflies when searching for food, during the summer period the monarch butterfly population begins a peregrination from North America to the south, and from the southern region of Canada to Mexico to seek subsistence, the same applies to butterflies who, through their senses, can monitor food sources and to have a mating partner for lineage continuity, the most common sense used by them is the smell, the one that directs them to get all the information they need about their trip. Each butterfly generates an odour according to its position, once another butterfly detects an odour and moves towards it, this detection is done in two ways: the first is called the global search and the second is called random search, where the butterfly randomly searches for areas where it can detect odours from other populations, for the movement of butterflies to be optimal; restricted steps are necessary such that; the whole population must give off a scent, each butterfly moves at random and the capacity of the stimulus depends on the place, environment where it is located and the objective sought [38]. The algorithm of Butterfly optimization technique is described below:

Butterfly optimization algorithm

Generate initial population of n butterflies w_i $(i = 1,2,\ldots,n)$
Simulate intensity I_i at w_i is determined by $f(w_i)$
Define sensor modality c, power exponent a and switch probability p
while stopping criteria not met **do**
  for each butterfly bf in population **do**
    Calculate fragrance for bf using equation $(f = cI^a)$
  end for
  Find the best bf (g^*)
  for each butterfly bf in population **do**
    Generate a random number r from [0,1]
    if $r < p$ **then**
      Move towards best butterfly/solution using equation $(w_i{}^{t+1} = w_i{}^t + (r^2 \times g^* - w_i{}^t) \times f_i)$
    Else
      Move randomly using equation $(w_i{}^{t+1} = w_i{}^t + (r^2 \times w_j{}^t - w_k{}^t) \times f_i)$
    end if
  end for
  Update the value of a
end while
Output the best solution found.

In order to conduct a comparison study with suggested BOA, one may consult other works related to other optimization techniques such as social spider optimization algorithm (SSO), Spider monkey optimization (SMO), cuckoo optimization algorithm (COA), Sine-cosine algorithm, Grey Wolf Optimize (GWO), Particle Swam Optimization (PSO), Whale Optimization Algorithm (WOA) [39-45].

5. Computer Simulation

In this section, the effectiveness of optimal LADRC and optimal NADRC has been evaluated via numerical simulation using MATLAB programming software. The numerical simulation has used Ode45 as a numerical solver. In addition, the simulation is based on the following assumptions:

i. The roll angle can operate within the allowable range ±30 degree,
ii. The uncertainty is unmatched disturbance, and it actually represents a gust wind, which can be simulated as a uniform random signal with upper and lower bounds $-10^o \leq \zeta(t) \leq 10^o$.
iii. The numerical values of parameters for wing-rock motion are given as [10]:
iv. $b_1 = -0.018$, $b_2 = 0.015$, $b_3 = -0.062$, $b_4 = 0.009$, $b_5 = 0.021$, $b_6 = 0.75$
v. The optimization algorithm based on BOA results in optimal design parameters for LADRC and NADRC

The optimization technique is responsible for tuning five design parameters, represented by k_1, k_2, b_0, h, R, and w_o for LADRC and twelve design parameters, represented by c_1, c_2, α_1, α_2, δ, b_0, h, R, β_1, β_2, β_3, and c for NADRC. The Root Mean Square Error (RMSE) has been chosen as the cost function (fitness function) and the minimization of cost function has been adopted in this optimization problem. The setting of design parameters-based BOA is listed in Table 1.

Table 1. The optimal values of design parameters for Optimal LADRC and Optimal NADRC based on BOA.

Design constants for NADRC	Value	Design constants for LADRC	Value
$\boldsymbol{c_1}$	215.23	$\boldsymbol{\beta_2}$	283.555
$\boldsymbol{c_2}$	42.48	$\boldsymbol{\beta_3}$	0.967
$\boldsymbol{\alpha_1}$	0.961	$\boldsymbol{c}$	67.006
$\boldsymbol{\alpha_2}$	0.898	k_1	499.999
$\boldsymbol{\delta}$	88.0243	k_2	28.946
$\boldsymbol{b_0}$	0.829	b_0	0.7478
$\boldsymbol{h}$	0.907	h	0.9067
$\boldsymbol{R}$	12.054	R	12.0539
$\boldsymbol{\beta_1}$	31.408	w_o	698.37

In this study, two scenarios have been taken into account; one is based on disturbance-free case, while the other scenario considered the exertion of disturbance on the aircraft.

Figure 2 shows the behaviours of roll angle for the disturbance-free case based on both proposed controllers. It is evident that the LADRC better enhances the

performance as compared to NADRC. The performances of proposed controllers are numerically evaluated and reported in Table 2. The RMS has been chosen as the index for performance evaluation.

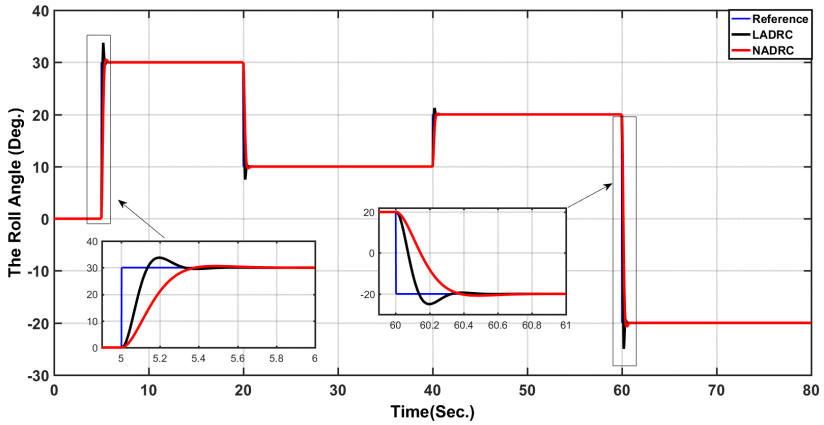

Fig. 2. The responses of roll motion due to LADRC and NADRC.

Table 2. Transient parameters of the controlled system based on LADRC and NADRC.

Controller Type	RMSE
LADRC	0.7931
NADRC	1.1067

Figure 3 shows the change rate of roll angle. The control effort due to LADRC and NADRC is indicated in Fig. 4. It is evident from the figure that the control signal in case of LADRC is higher than that in case of NADRC. However, this is the price paid by the optimal controller to enhance or improve the dynamic performance of the optimal controlled wing-rock motion. The behaviors of error signal for optimal controllers are shown in Fig. 5.

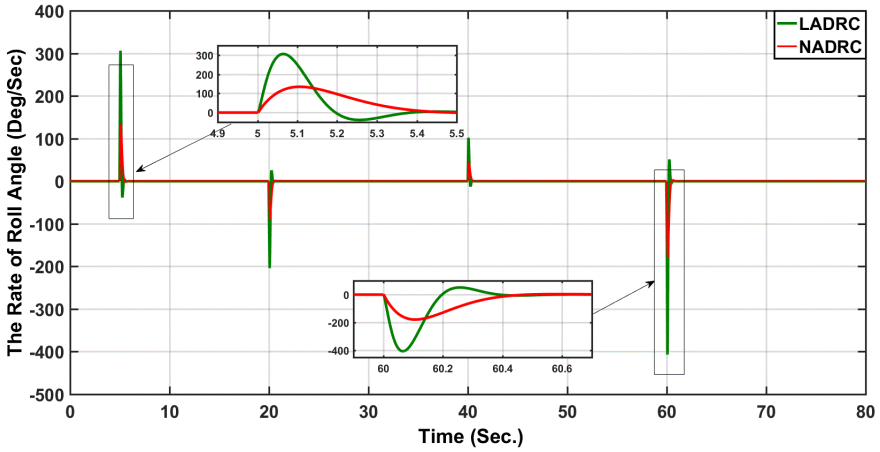

Fig. 3. The rate change of roll angle.

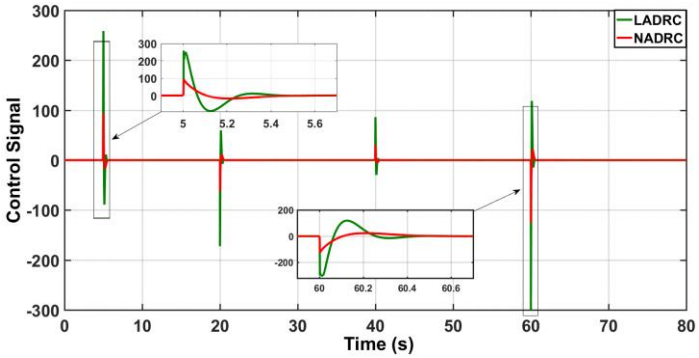

Fig. 4. The control effort due to both LADRC and NADRC.

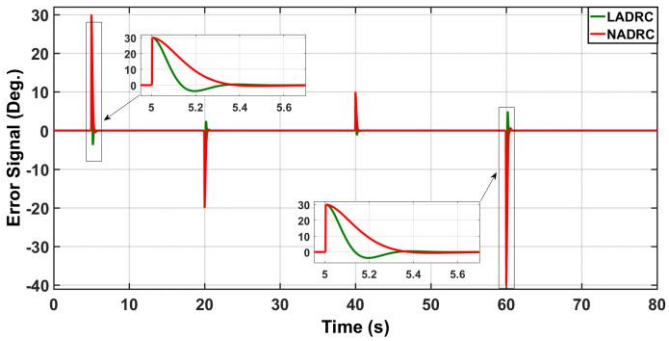

Fig. 5. The error signal due to both LADRC and NADRC.

In the next scenario, the disturbance due to wind gust is taken into account and the performances of LADRC and NADRC are evaluated based on computer simulation. The behaviour of applied disturbance is described in Fig. 6. As mentioned earlier, the disturbance lies within the range $-10^o \leq \zeta(t) \leq 10^o$ and has uniform random distribution such that it is mimicking the real wind-gust. The response of roll motion based on optimal controllers in the presence of wind disturbance has been illustrated in Fig. 7. The disturbance has been exerted in specified periods of time and the figure shows that the LADRC shows good dynamic performance under the applied disturbance.

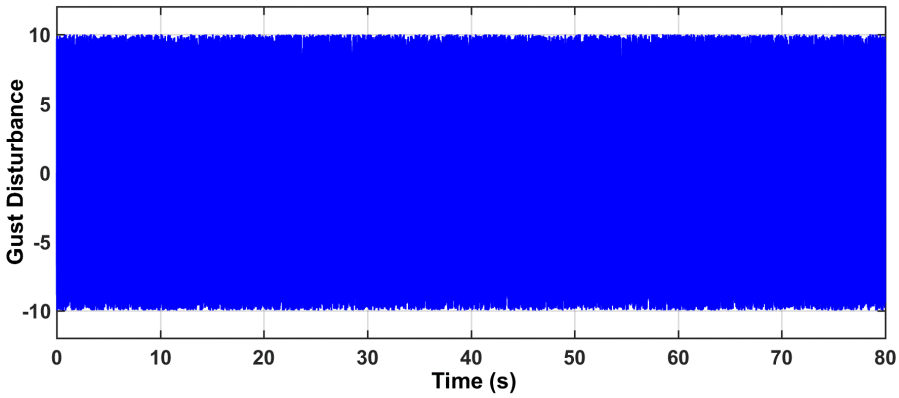

Fig. 6. The disturbance behaviour of wind gust.

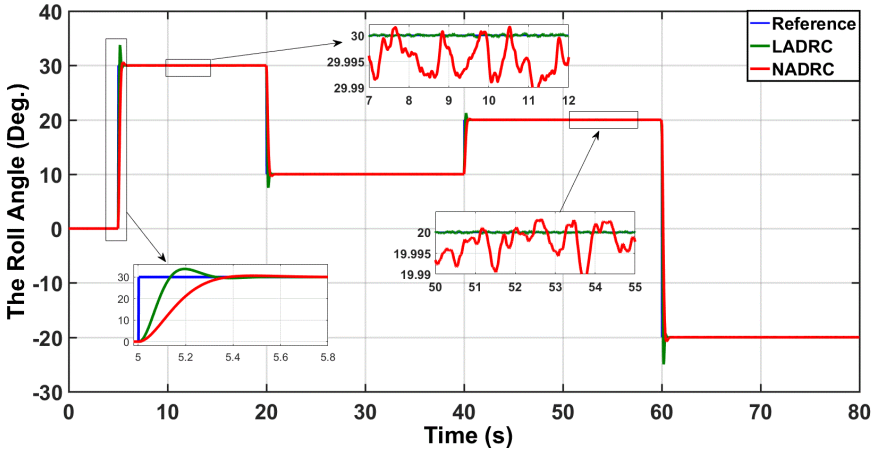

Fig. 7. The roll motion subjected to disturbance.

Figures 8 and 9 show the rate change of roll motion and control effort, respectively, under the action of disturbance.

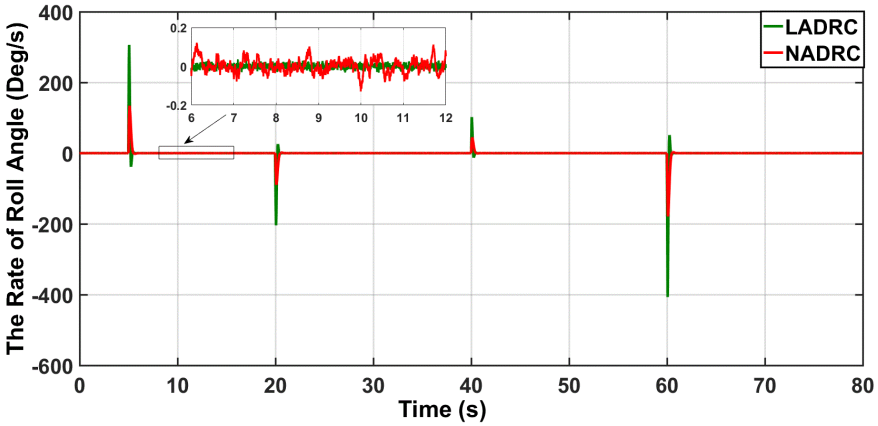

Fig. 8. The rate change of roll motion under disturbance.

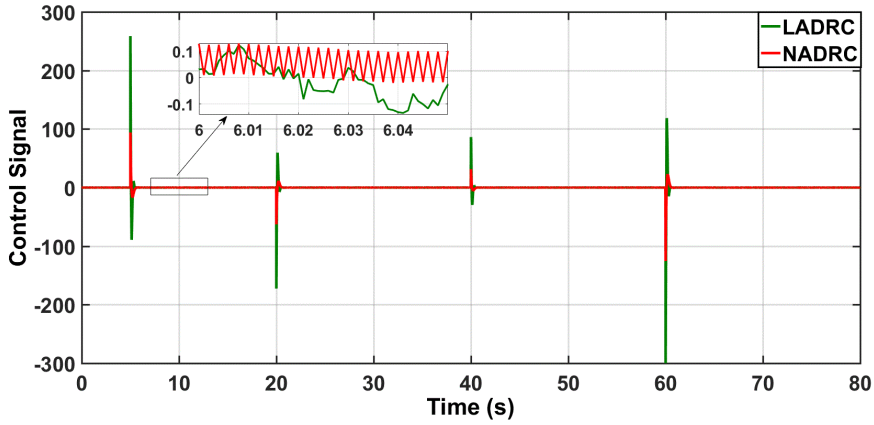

Fig. 9. The control effort of LADRC and NADRC in the presence of disturbance.

This study can be extended for future work by proposing other control strategies to address the wing-rock phenomena and to evaluate their performances compared to the ADRC and to demonstrate their effectiveness in terms of rejection capabilities against this flight unwanted behaviour [46-60].

6. Conclusion

In this study, the LADRC and NADRC have been developed to control the wing-rock motion of delta-wing aircraft. The BOA has been applied to tune the design parameters of the controllers in order to have optimal performance of proposed controllers. The optimal LADRC based on BOA is compared to that based on optimal NADRC via computer simulation within MATLAB environment. The simulated results showed optimal LADRC outperforms the optimal NADRC in terms of transient and steady state characteristics.

Nomenclatures

b	The chord of the wing
b_1, b_2, b_3, b_4, b_5	Unknown constants
D	The effectiveness rolling of differential ailerons rolling
$f(x, w, t)$	Unknown nonlinear term
h	The sampling period
I_{xx}	The wing moment of inertia around the roll span axis
P	Positive definite matrix
S	The wing area of aircraft
U^{∞}	The speed of free air stream
u	Control law
w_i	Initial population of butterfly
x_1, x_2, x_3	Actual state variables
$\hat{x}_1, \hat{x}_2, \hat{x}_3$	Estimated state variables
$\tilde{x}_1, \tilde{x}_2, \tilde{x}_3$	Estimation errors

Greek Symbols

ϕ	Roll angle
ρ	The air density
$\zeta(t)$	The non-parametric uncertainty (gust or storm wind)

Abbreviations

ADRC	Active disturbance rejection control
BOA	Butterfly Optimization Algorithm
COA	Cuckoo optimization algorithm
ESO	Extended State Observer
GWO	Grey wolf optimizer
LADRC	Linear active disturbance rejection control
NADRC	Nonlinear active disturbance rejection control
SMO	Spider monkey optimization
SSO	Social spider optimization algorithm
STESO	Super-twisting Extended-State Observer
TD	Tracking differentiator
WOA	Wale Optimization Algorithm

References

1. Kooi, S.B.L. (1999). *Dynamic recurrent neural networks for stable adaptive control of wing rock motion*. Ph.D. Thesis. Concordia University, Montréal, Québec, Canada.
2. Saleh, M.H.; Al-Qassar, A.A.; Othman, M.Z.; and Al-Obaidi, A.S.M. (2010). Development of the cross-coupling phenomena of MIMO flight system using fuzzy logic controller. *Journal of Engineering Science and Technology* (*JESTEC*), 5(1), 85-93.
3. Al-Qassar, A.A.; Al-Dujaili, A.Q.; Hasan, A.F.; Humaidi, A.J.; Ibraheem, I.K.; and Azar, A.T. (2021). Stabilization of single-axis propeller-powered system for aircraft applications based on optimal adaptive control design. *Journal of Engineering Science and Technology* (*JESTEC*), 16(3), 1851-1869.
4. Al-Qassar, A.A.; Al-Obaidi, A.S.M.; Hasan, A.F.; Humaidi, A.J.; Ibraheem, K.I., Azar, A.T.; Hameed, A.H. (2021). Grey-wolf optimization better enhances the dynamic performance of roll motion for tail-sitter VTOL aircraft guided and controlled by STSMC. *Journal of Engineering Science and Technology* (*JESTEC*), 16(3), 1932-1950.
5. Castellanos, J.C.; Suárez F.C.; and Sofrony, E.J. (2021). Review of L1 adaptive control for solving the wing rock problem. *Journal of Engineering and Applied Sciences*, 16(9), 296-303.
6. Ignatyev, D.I. (2018). Neural network adaptive control of wing-rock motion of aircraft model mounted on three-degree-of-freedom dynamic rig in wind tunnel. *Progress in Flight Dynamics, Guidance, Navigation, and Control*, 10(2018). 73-86.
7. Gonz´alez, A.;and Ra´ul, O. (2005). Adaptive control scheme for plants with time-varying structure using on-line parameter estimation. *Proceedings of the* 44*th IEEE Conference on Decision and Control, and the European Control Conference*. Seville, Spain, December 12-15, 2005, 2225-2229.
8. Steven, B.L.; and Svoboda, J.V. (1998). Dynamic recurrent neural networks for stable adaptive control of wing rock motion. *IFAC Proceedings Volumes*, 31(21), 231-236.
9. Guglieri, G.; and Satori, D. (2013). Design of a sliding mode control for wing rock suppression in highly-swept wing aircraft. *International Journal of Aerospace Sciences*, 2(1), 1-10.
10. Humaidi, A.J.; and Hameed, A.H. (2017). Robust MRAC for a wing rock phenomenon in delta wing aircrafts. *AUT Journal of Modeling and Simulation*, 49(1), 113-122.
11. Liu, Z.L.; and Su, C.Y. (2004). Control of wing rock phenomenon with a variable universe fuzzy controller. *Proceeding of the* 2004 *American Control Conference*. Boston, Massachusetts June 30-July 2, 2004, 1719-1724.
12. Al-Qassar, A.A.; Al-Obaidi, A.S.M.; Hasan, A.F.; Humaidi, A.J.; Nasser, A.R.; Alkhayyat, A.; and Ibraheem K.I. (2021). Finite-time control of wing-rock motion for delta wing aircraft based on whale-optimization algorithm. *Indonesian Journal of Science & Technology*, 6(3), 441-456.
13. Wu, D.; Chen, M.; Gong, H.; and Wu, Q. (2017). Robust backstepping control of wing rock using disturbance observer. *Applied Science*s, 2017, 7, 219, 1-29.

14. Roshanian, J.; and Rahimzadeh, E. (2020). A generalization for model reference adaptive control and robust model reference adaptive control adaptive laws for a class of nonlinear uncertain systems with application to control of wing rock phenomenon. *International Journal of Engineering, Transaction B: Applications*, 33(11), 2372-2383.
15. Humaidi, A.J.; Hameed, A.H.; Ibraheem, K.I. (2019). Design and performance study of two sliding mode backstepping control schemes for roll channel of delta wing aircraft. 2019 6*th International Conference on Control, Decision and Information Technologies* (*CoDIT*). France, Paris, 23-26 April, 1215-1220.
16. Alawad, N.A.; Humaidi, A.J.; Al-Araji A.S. (2022). Improved active disturbance rejection control for the knee joint motion model. *Mathematical Modelling of Engineering Problems*, 9(2), 477-483.
17. Alawad, N.A.; Humaidi, A.J.; Al-Obaidi, A.S.M.; Al-Araji A.S. (2022). Active disturbance rejection control of wearable lower-limb system based on reduced ESO. *Indonesian Journal of Science & Technology*, 7(2), 203-218.
18. Abdul-Adheem, W.R.; Azar, A.T.; Ibraheem, I.K.; Humaidi, A.J. (2020). Novel active disturbance rejection control based on nested linear extended state observers. *Applied Sciences*, 10, 4069.
19. Han, J. (2009). From PID to active disturbance rejection control. *IEEE Transactions on Industrial Electronics*, 56(3), 900-906.
20. Gao, Z. (2003). Scaling and bandwidth-parameterization based controller tuning. *Proceedings of the* 2003 *American Control Conference*. Denver, CO, USA, 04-06 June, 4989-4996.
21. Wei, Z.; Aiguo, S. (2020). Active motion control of a knee exoskeleton driven by antagonistic pneumatic muscle actuators. *Actuators*, 9(4), 1-14.
22. Zhu, E.; Pang, J.; Sun, N.; Gao, H.; Sun, Q.; Chen, Z. (2013). Airship horizontal trajectory tracking control based on active disturbance rejection control (ADRC). *Nonlinear Dynamic*, 75(4), 725-734.
23. Long, Y.; Du, Z.; Cong, L.; Wang, W.; Zhang, Z.; Dong, W. (2017). Active disturbance rejection control based human gait tracking for lower extremity rehabilitation exoskeleton. *ISA Transactions*, 67, 389-397.
24. Chen, C.; Du, Z.; Dong, W. (2019). Active disturbance rejection with fast terminal sliding mode control for a lower limb exoskeleton in swing phase. *IEEE Access*, 7, 72343-72357.
25. Humaidi, A.J.; Badr, H.M. (2018). Linear and nonlinear active disturbance rejection controllers for single-link flexible joint robot manipulator based on PSO tuner. *Journal of Engineering Science and Technology Review*, 11(3), 133-138.
26. Humaidi, A.J.; Badr, H.M.; Ajel, A.R. (2018). Design of active disturbance rejection control for single-link flexible joint robot manipulator. 2018 22*nd International Conference on System Theory, Control and Computing* (*ICSTCC*). Sinaia, Romania, 10-12 Oct., 452-457.
27. Humaidi, A.J.; Badr, H.M.; Hameed, A.H. (2018). PSO-based active disturbance rejection control for position control of magnetic levitation system. 2018 5*th International Conference on Control, Decision and Information Technologies* (*CoDIT'*18). Thessaloniki, Greece, April 10-13, 922-928.

28. Arora, S.; and Singh, S. (2019). Butterfly optimization algorithm: A novel approach for global optimization. *Soft Computing*, 23, 715-734.
29. Assiri, A. (2021). On the performance improvement of Butterfly Optimization approaches for global optimization and Feature Selection. *PLoS ONE*, 16, 1-27.
30. Utama, D.M.; Widodo, D.S.; Ibrahim, M.F.; and Shanty, K.D. (2020). A new hybrid butterfly optimization algorithm for green vehicle routing problem. *Journal of Advanced Transportation*, Volume 2020, ID 8834502, 1-14.
31. Li, G.; Shuang, F.; Zhao, P.; Le, C. (2019). An improved butterfly optimization algorithm for engineering design problems using the cross-entropy method. *Symmetry*, 11, 1049.
32. Tarun K.S.; Ashok, K.S.; and Goyal, P. (2021). Bidirectional butterfly optimization algorithm and engineering applications. *Materials Today: Proceedings*, 34(3), 736-741.
33. Al Hamami, D.J.; Al Gburi, H.Q.; Al Baiati, A.E. (2021). Path-planning in 3D space using butterfly optimization algorithm. *Periodicals of Engineering and Natural Sciences*, 9(2), 365-374.
34. Bin, Li.; Chao, L.; Huaning, W.; Yifeng, Z.; Yinghui, D. (2019). Chaotic adaptive butterfly mating optimization and its applications in synthesis and structure optimization of antenna arrays. *International Journal of Antennas and Propagation*, Vol. 2019, Article ID 1730868, 1-14.
35. Hsu, C.; and Lan, C.E. (1985). Theory of wing rock. *Journal of Aircraft*, 22(10), 920-924.
36. Guglieri, G. (2012). A comprehensive analysis of wing rock dynamics for slender delta wing configurations. *Nonlinear Dynamics*, 69, 1559-1575.
37. Elzebda, J.M.; Nayfeh A.H.; and Mook D.T. (1989). Development of an analytical model of wing rock for slender delta wings. *Journal of Aircraft*. 26(8), 737-743.
38. Zhang, M.; Long, D.; Qin, T.; Yang, J. (2020). A chaotic hybrid butterfly optimization algorithm with particle swarm optimization for high-dimensional optimization problems. *Symmetry*, 12, 1800.
39. Humaidi, A.H.; Najem, H.T.; Al-Dujaili, A.Q.; Pereira, D.A.; Ibraheem, I.K.; Azar, A.T. (2021). Social spider optimization algorithm for tuning parameters in PD-like interval type-2 fuzzy logic controller applied to a parallel robot. *Measurement and Control*, 54(3-4), 1-21.
40. Al-Azza, A.A.; Al-Jodah, A.A.; and Harackiewicz, F.J. (2015). Spider monkey optimization: A novel technique for antenna optimization. *IEEE Antennas and Wireless Propagation Letters*, 15, 1016-1019.
41. Moezi, S.A.; Zakeri, E.; and Zare, A. (2018). A generally modified cuckoo optimization algorithm for crack detection in cantilever Euler-Bernoulli beams. *Precision Engineering*, 52, 227-241.
42. Mirjalili, S. (2016). SCA: A sine cosine algorithm for solving optimization problems. Knowledge-Based Systems, 96, 120-133.
43. Humaidi, A.J; Kadhim, S.K; Gataa, A.S. (2021). Optimal adaptive magnetic suspension control of rotary impeller for artificial heart pump. *Cybernetics and Systems*, 53(1), 141-167.

44. Humaidi, A.J.; Kadhim, S.K.; Gataa, A.S., (2020). Development of a novel optimal backstepping control algorithm of magnetic impeller-bearing system for artificial heart ventricle pump. *Cybernetics and Systems*, 2020, 51(4), 521-541.
45. Ghanim, T.; Ajel, A.R.; Humaidi, A.J. (2020). Optimal fuzzy logic control for temperature control based on social spider optimization. *IOP Conference Series: Materials Science and Engineering*, 745(1), 012099.
46. Humaidi, A.J.; and Hameed, A.H. (2018). PMLSM position control based on continuous projection adaptive sliding mode Controller. *Systems Science & Control Engineering*, 6(3), 242-252.
47. Hameed, A.H; Al-Dujaili, A.Q.; Humaidi, A.J.; and Hussein, H.A. (2019). Design of terminal sliding position control for electronic throttle valve system: A performance comparative study. *International Review of Automatic Control* (I.RE.A.CO.), 12(5), 251-260.
48. Humaidi, A.J.; Hasan, S.; Al-Jodah, A.A. (2018). Design of second order sliding mode for glucose regulation systems with disturbance. International Journal of Engineering and Technology (UAE), 7 (2), 243–247.
49. Humaidi, A.J.; Hameed, A.H. (2017). Robustness enhancement of MRAC using modification techniques for speed control of three phase induction motor. *Journal of Electrical Systems*, 2017, 13(4), 723-741.
50. Hassan, M.Y.; Humaidi, A.J.; Hamza, M.K. (2020). On the design of backstepping controller for acrobot system based on adaptive observer. *International Review of Electrical Engineering*, 15(4), 328-335.
51. Humaidi, A.J.; Abdulkareem, A.I. (2019). Design of augmented nonlinear PD controller of Delta/Par4-like robot. *Journal of Control Science and Engineering*, Volume 2019 |Article ID 7689673.
52. Humaidi, A.J.; Hameed, M.R. (2017). Design and performance investigation of block-backstepping algorithms for ball and arc system. 2017 *IEEE International Conference on Power*, *Control*, *Signals and Instrumentation Engineering* (*ICPCSI*). Chennai, India, 21-22 September, 325-332.
53. Abed, H.Y.; Humod, A.T.; Humaidi, A.J. (2020). Type 1 versus type 2 fuzzy logic speed controllers for brushless DC motors. *International Journal of Electrical and Computer Engineering*, 10(1), 265-274.
54. Humaidi, A.J.; Talaat, E.N.; Hameed, M.R.; Hameed, A.H. (2019). Design of adaptive observer-based backstepping control of cart-pole pendulum system. 2019 *IEEE International Conference on Electrical*, *Computer and Communication Technologies* (*ICECCT*). Coimbatore, India, 20-22 February 2019, 1-5.
55. Humaidi, A.J.; Hameed, A.H.; Hameed, M.R. (2018). Robust adaptive speed control for DC motor using novel weighted E-modified MRAC. 2017 *IEEE International Conference on Power*, *Control*, *Signals and Instrumentation Engineering* (*ICPCSI*). Chennai, India, 21-22 September, 313-319.
56. Humaidi, A.J.; Hameed, A.H. (2019). Design and comparative study of advanced adaptive control schemes for position control of electronic throttle valve. *Information* (*Switzerland*), 10(2), 65.
57. Humaidi, A.J.; Hameed, M.R.; Ajel, A.R.; Hameed, A.H.; Al-Qassar, A.A.; Ibraheem, I.K. (2021). Block backstepping control design of two-wheeled

inverted pendulum via zero dynamic analysis. 2021 *IEEE* 12*th Control and System Graduate Research Colloquium* (*ICSGRC*). Shah Alam, Malaysia, 87-92.

58. Humaidi, A.J.; and Hussein, H.A. (2019). Adaptive control of parallel manipulator in cartesian space. 2019 *IEEE International Conference on Electrical*, *Computer and Communication Technologies* (*ICECCT*). Coimbatore, India, 20-22 February, 1-8.
59. Mahdi, S.M.; Yousif, N.Q.; Oglah, A.A.; Sadiq, M.E.; Humaidi, A.J.; Azar, A.T. (2022). Adaptive synergetic motion control for wearable knee-assistive system: A rehabilitation of disabled patients. *Actuators*, 11(7), 176.
60. Aljuboury, A.S.; Hameed, A.H.; Ajel, A.R.; Humaidi, A.J.; Alkhayyat, A.; Mhdawi, A.K.A. (2022). Robust adaptive control of knee exoskeleton - assistant system based on nonlinear disturbance observer. *Actuators*, 11(3), 78.